Journal Pre-proofs

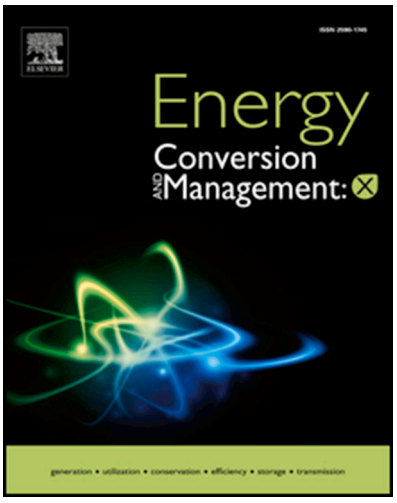


# Comparative examinations of wind speed and energy extrapolation methods using remotely sensed data – A case study from Hungary

István Lázár, István Hadnagy, Boglárka Bertalan-Balázs, László Bertalan, Sándor Szegedi

PII: S2590-1745(24)00238-1
DOI: https://doi.org/10.1016/j.ecmx.2024.100760
Reference: ECMX 100760

To appear in: *Energy Conversion and Management: X*

Received Date: 1 July 2024
Revised Date: 27 September 2024
Accepted Date: 13 October 2024

Please cite this article as: I. Lázár, I. Hadnagy, B. Bertalan-Balázs, L. Bertalan, S. Szegedi, Comparative examinations of wind speed and energy extrapolation methods using remotely sensed data – A case study from Hungary, *Energy Conversion and Management: X* (2024), doi: https://doi.org/10.1016/j.ecmx.2024.100760

# Comparative examinations of wind speed and energy extrapolation methods using remotely sensed data – A case study from Hungary

István Lázár[a], István Hadnagy[b], Boglárka Bertalan-Balázs[c,*], László Bertalan[d], Sándor Szegedi[e]

[a] Department of Meteorology, University of Debrecen, H-4032 Egyetem tér 1. Debrecen, Hungary
e-mail: lazar.istvan@science.unideb.hu, ORCID: 0000-0003-0247-2282

[b] Department of Biology and Chemistry, Ferenc Rákóczi II Transcarpathian Hungarian College of Higher Education, UA- 90200 Kossuth square, 6. Beherove, Ukraine
e-mail: hadnagy.istvan@kmf.org.ua, ORCID: 0000-0001-8931-4863

[c*] Corresponding author. Department of Physical Geography and Geoinformatics, University of Debrecen, H-4032 Egyetem tér 1. Debrecen, Hungary
e-mail: balazs.boglarka@science.unideb.hu , ORCID: 0000-0003-0605-2891

[d] Department of Physical Geography and Geoinformatics, University of Debrecen, H-4032 Egyetem tér 1. Debrecen, Hungary
e-mail: bertalan@science.unideb.hu , ORCID: 0000-0002-5963-2710

[e] Department of Meteorology, University of Debrecen, H-4032 Egyetem tér 1. Debrecen, Hungary
e-mail: szegedi.sandor@science.unideb.hu

**Abstract**

Exact knowledge of wind energy potential is a fundamental issue in wind energy utilization. The vertical changes in wind speeds, that is, the wind profile, have a predominant impact on the wind energy available at a location because the kinetic energy of moving air is proportional to the square of the wind speed. Roughness describes the resistance of a 3D surface to moving air. The exponent α of the power law of Hellmann and the roughness length ($z_0$) are two parameters that describe the effects of the roughness of the surface on the wind profile. They can be used for the vertical extrapolation of wind speeds. The exponent α can be determined using multiple height level wind speed measurement data, whereas a reliable technique for the calculation of the roughness length requires detailed knowledge of the 3D geometry of the measurement site. In the present study, the exponent α was calculated based on SODAR wind speed measurements, while ($z_0$) was determined using a combination of GIS and UAS-based aerial survey methods. Wind speeds measured at 50 m were extrapolated for height levels of 80, 90, 100, 110, and 120 m using dynamic power law exponent values. Wind power was determined using the power law (method V1), roughness length (method V2), frequency distribution (method W-RF), and gamma distribution (method W-G), and Windographer software was compared to the values calculated from the empirical (measured) wind speeds. A comparative statistical analysis of the datasets of the power law and roughness length methods on monthly/diurnal, annual/diurnal, and month/direction contexts showed no significant differences at all height levels. Differences can be detected in the distribution of the signs of the differences at heights of 80 and 120 m for the entire dataset. Underestimation was dominant with a significant frequency (over 70%) in the case of both methods and heights. There were no significant differences between the wind power estimations provided by the different methods, and all the methods involved in the study underestimated the wind speeds and wind energy potential for each height level. Methods V1 and V2 can be used alternatively, depending on the input data available for analysis. The major advantage of method V2 is that it provides the same accuracy as V1, which requires a UAS-based aerial survey at the beginning, but continuous wind measurements must be performed at a lower height only. This means that there is no need for a high measurement tower, which makes the measurements simpler, more cost-effective, and causes much less disturbance

to the environment. Another important advantage of the methods presented here is that they use a dynamic approach of power law exponent values that provide a more realistic estimation of wind speed and energy on a diurnal scale.

**Keywords:** wind profile, remote sensing, power law, roughness length, Weibull distribution, wind energy potential estimation

## 1. Introduction

The changes in wind speed with height, that is, the wind profile, have great importance in several practical fields, from wind erosion [1] through urban climate (aerodynamics of urban areas [2]; roughness mapping and modelling in urban areas [3,4]; roughness parametrization [5]; urban heat island effect [6,7]) and air pollutant dispersion [8–10] to wind energy utilization (energy production [11,12], wind modelling [13,14], potential assessment [15–17], turbine technology [18,19], and Weibull distribution [20,21]).

Exact knowledge of wind energy potential is a fundamental issue in wind energy utilization. The vertical changes in wind speeds have a predominant impact on the wind energy available at a location because the kinetic energy of the moving air is proportional to the square of the wind speed. The wind speeds show strong horizontal and vertical fluctuations over the surface. The hub height of wind turbines is between 80 and 120 m, whereas wind speed measurements usually take place between 10 and 50 m. Thus, it is fundamental to estimate wind speeds for the hub height of wind turbines from data measured at lower heights in wind energy utilization. There are different methods for this type of vertical extrapolation of wind speeds, which require different input data and provide different levels of accuracy.

For this reason, the main aim of the present study is to provide information that helps select between the methods available for vertical extrapolation of wind speeds via a comprehension of measured (empirical) wind speeds at different heights and data estimated for those heights using different vertical extrapolation methods.

The friction between the layers of the moving air masses and the surface has a principal effect on the wind profile. Different parameters are used to describe the resistance of a 3D surface against moving air, such as the surface roughness, roughness [13,22], and wind shear coefficient [23]. The roughness of the surface has a fundamental impact on wind speeds within the boundary layer. Therefore, the roughness must be considered in the calculation of wind speeds at different heights over the surface.

There are several methods for determining the wind profile, from relatively simple to highly complex methods, such as the logarithmic wind profile of the Deacon or the power law equation [9,22,24]. One of the most frequently used methods for determining the wind profile is the Hellmann power law equation.

The roughness varied significantly as a function of the surface geometry. It is determined by the type of surface cover, relief, and objects on the surface [1] on one hand, meteorological conditions in the boundary layer (temperature, stability, moisture, air pressure, density, turbulence, vertical wind shear, etc.) have a remarkable impact on it on the other hand [12,25,26]. Due to these effects, it varies across different sites and has a diurnal and annual course [22,23,27]. On this basis, many researchers have dealt with the effects of atmospheric stability conditions on the exponent α of the power law, which corresponds to the roughness of the surface [11,23,25].

Another important parameter in the equations that describes the changes in wind speed with height is the roughness length ($z_0$). The roughness length at a given site decreases with increasing wind speed [1]. It is highly influenced by the relief formed by the 3D objects on the surface (in this context, roughness elements). Over a surface composed of higher roughness elements, the roughness length will be higher (WMO Guide). Its value is determined by the ratio of the area to the width of a given roughness element facing wind [28]. In addition, the flexibility of the roughness elements has a significant impact. If wind can deform the elements, as in the case of grass, their height can decrease, resulting in a decrease in roughness length [1].

There are three main groups of methods for calculating roughness length [1,3,13]:

- geometric methods which use measures of surface morphometry.
- roughness classification methods that use roughness classes combined with visual estimation.

- micrometeorological methods which use wind measurement data.

The most common micrometeorological method uses wind speed data from wind measurement towers observed at different heights [3].

There are a wide variety of statistical methods for the vertical extrapolation of wind speeds and estimation of available wind power with different input data requirements, which makes the selection between the methods quite complicated in wind energy utilization practice. Therefore, our study aimed to achieve three primary objectives. First, we assessed commonly utilized techniques for the vertical extrapolation of wind speed data. This involves understanding the measured and estimated wind speeds through the application of the power law equation (method V1) and roughness length (method V2). Our method uses a dynamical approach to provide a better description of the power law exponent, which exhibits strong spatial and temporal variability. Second, we sought to determine the roughness length using data collected from a UAS-based aerial survey employing the frontal area index (FAI). Finally, we aimed to compare various methods for estimating the wind energy potential. These include the use of estimated wind speeds via the power law (method V1) and roughness length (method V2), as well as techniques such as frequency distribution (method W-RF), gamma distribution (method W-G), and Windographer software against empirically measured wind speeds. In this study, we performed comparative calculations of the difference in the estimated specific wind energy potential caused by the results of different extrapolation methods. In addition to the extrapolated data, the comparison was based on wind speed values measured by remote sensing at the same altitudes. Our aim is to offer a satisfactory alternative for wind energy assessment in areas with different terrains, technical backgrounds, and cost coverage, taking into account the available tools and methods.

## 2. Materials and methods

The wind speed datasets used in the present study were provided by a METEK PCS.2000-24 type SODAR (SOund Detection And Ranging) instrument owned by the Faculty of Science and Technology, University of Debrecen, Hungary, and managed by the Department of Meteorology, University of Debrecen, Hungary. The instrument is situated at the Agrometeorological Observatory of the University; elevation above sea level is 125 m) (Fig. 1). . The study area is ideal for this type of examination because it is situated on flat terrain surrounded by diverse environments (built-up patches, croplands, forest spots, and wetlands). As it is the Agrometeorological Observatory of the University of Debrecen and the SODAR instrument is mounted there, all meteorological data required for the analysis are available for the site. The SODAR instrument can determine wind speed and direction using the reflection of sound waves from the density fluctuations of air in the lowest layer of the atmosphere [29]. The instrument emits (audible) sound waves at four frequencies: 1775 Hz, 1975 Hz, 2175 Hz, and 2375 Hz. It measures wind speeds within a height interval between 20 and 300 meters in 10-meter height steps in 1-minute time intervals and registers 10-minute averages. Our wind speed datasets consist of 150,000 records for each height level in the three years between 01/01/2016 and 31/12/2018 with no interruptions. The availability of data decreases with increasing height, so there is no data for 4.2% of the studied period at the height interval between 20 and 90 m, whereas there is a lack of data for 4.3% of the studied period between 100 and 120 m.

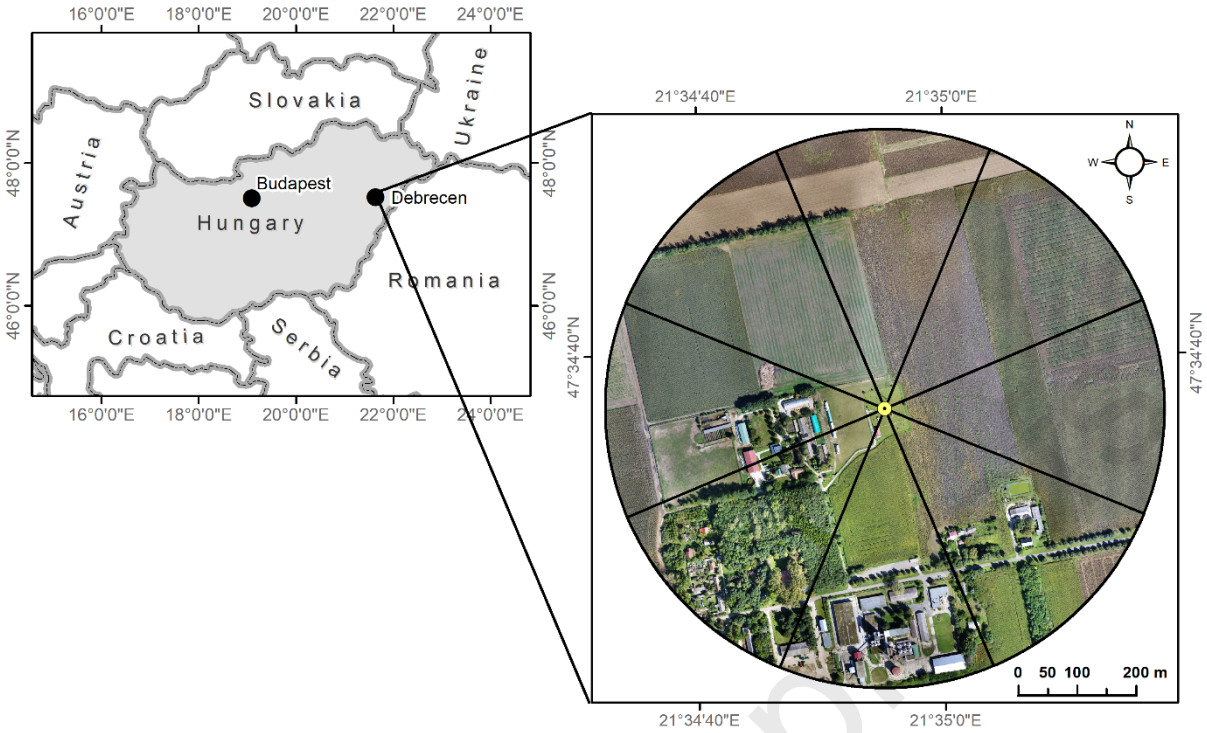


Fig. 1. Location of SODAR measurements.

Statistical analyses and data processing for visualization were performed using MS Excel. For graphic interpretation of the wind speeds measured by the SODAR instrument and those estimated along with the differences between the two datasets, the Surfer 12 software was used.

## 2.1 Methods for the vertical extrapolation of wind speeds

A comprehensive workflow of the analysis conducted within the scope of this study is illustrated in Fig.2. In the present study, two methods were compared for the estimation of wind speeds for typical hub height levels of wind turbines between 80 and 120 m with 10 m height steps.

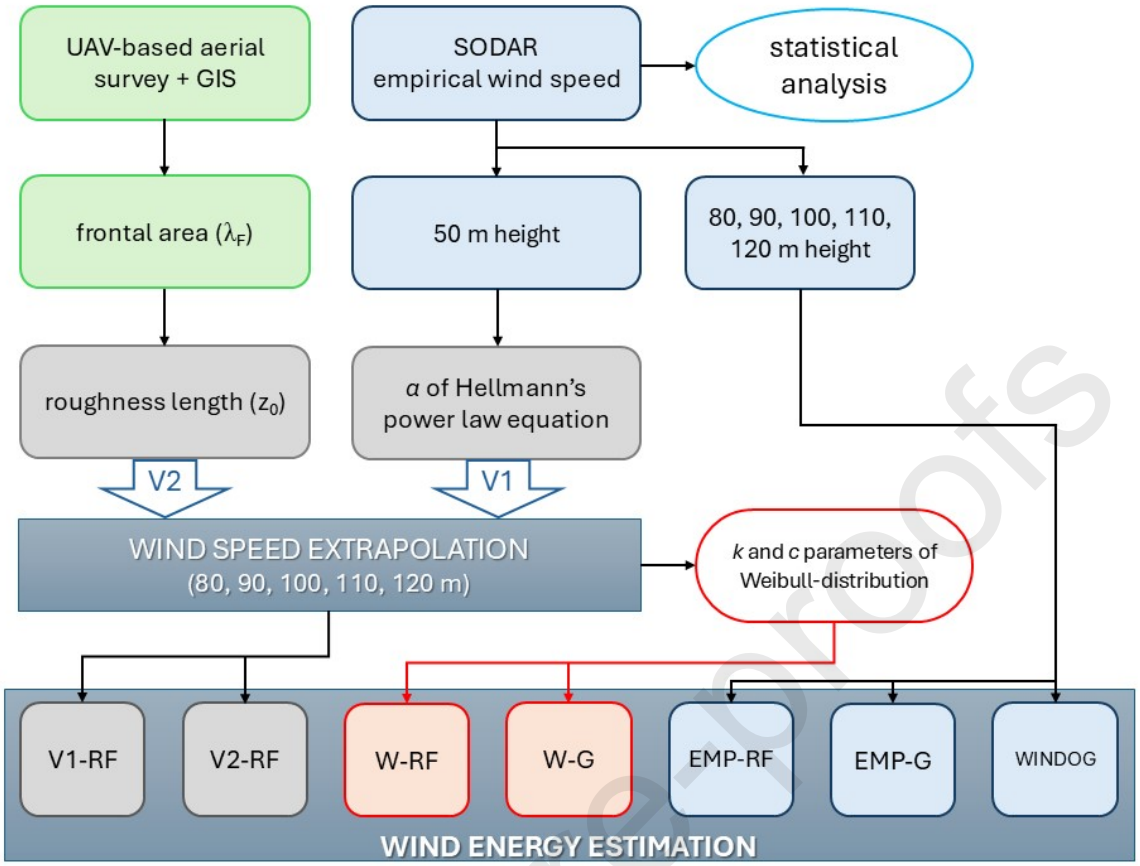


Fig. 2. The flowchart of the implemented analysis.

### 2.1.1 Power law exponent (method V1)

The power law equation of Hellmann, which is widely used in wind climatology [30–32], was applied first. The general form of the equation is

$$\frac{v_2}{v_1} = \left(\frac{h_2}{h_1}\right)^{\alpha} \qquad \text{(Eq. 1)}$$

where $v_1$ is the wind speed measured at height $h_1$ and $v_2$ is the wind speed measured at height $h_2$. The values of the exponent α are strongly influenced by the topography of the surface and stability conditions in the close-to-the-surface layer of the atmosphere [9,22,33], which results in a characteristic diurnal and annual course. This value can vary across a wide interval [34,35]. When temperatures are low close to the surface, under stable conditions, their values are high, whereas their values are low under unstable conditions when temperatures are high close to the surface [36]. Its values are higher at night, but the course is more regular during daytime hours [37].

The average values of exponent α over different surface cover types, based on the results of Master [38], are presented in Table 1. There were only slight differences between the categories, and some values did not belong to any one category. These values were intermittent between the categories. A more accurate

estimation can be achieved by extrapolating exponent α for heights over $h_2$ by considering one- or multiple-hour averages instead of one static average [39].

**Table 1.** Relationship between the values of the exponent α in the power law of Hellmann and surface cover types [38]

| **Type of surface cover** | ***values of α*** |
|---|---|
| Open water bodies, plain land surface | 0.10-0.12 |
| Grasslands, open land areas | 0.15-0.16 |
| High vegetation, bushes | 0.20-0.22 |
| Forest lowlands | 0.25-0.28 |
| Low-intensity buildup spaces (small town with extensive green spaces) | 0.30-0.35 |
| Heavy buildup spaces (cities with skyscrapers) | 0.40-0.50 |

In our study, the values of exponent α were calculated based on several measurement levels for each measured (empirical) $v_1$ and $v_2$ data pair [40–42]:

$$\alpha = \frac{ln\left(\frac{v_2}{v_1}\right)}{ln\left(\frac{h_2}{h_1}\right)} \qquad \text{(Eq. 2)}$$

Using the values of exponent α calculated from the empirical data pairs, wind speeds from height $h_2$ to the typical hub heights of the onshore wind turbines. Based on the above equations, $v_2$ can be expressed as follows [41,43,44].

$$v_2 = v_1\left(\frac{h_2}{h_1}\right)^{\alpha} \qquad \text{(Eq. 3)}$$

Wind speeds measured at 50 m were extrapolated for height levels of 80, 90, 100, 110, and 120 m using dynamic power law exponent values.

### 2.1.2 Vertical extrapolation of wind speeds using the roughness length (method V2)

The wind profile of the power law exponent of Hellmann is closely related to the logarithmic wind profile because its form, used in international engineering practice, is derived from the logarithmic wind profile [41]

$$\alpha = \frac{1}{ln\frac{10}{z_0}} \quad \text{(Eq. 4)}$$

Based on this relationship over a smooth surface ($z_0$=0,01 m), the exponent has a value of $\alpha$=1/7≈0.14, during the day, and $\alpha$=1/5≈0.2, during night hours [34,45,46]. Therefore, the values of $\alpha$ were affected by the roughness length ($z_0$).

On this basis, the value of the roughness length ($z_0$) wind speed at multiple height levels can be determined directly using the logarithmic wind profile [41,43,47]:

$$v_2 = v_1\left(\frac{ln\left(\frac{h_2}{z_0}\right)}{ln\left(\frac{h_1}{z_0}\right)}\right) \quad \text{(Eq. 5)}$$

**2.1.2.1 Estimation of the roughness length**

The roughness length ($z_0$) describes the collective hindering effect of the roughness elements on the surface against wind. It defines the height over the surface (the layer that acts as the surface for moving air) at which the wind speed becomes zero [48]. Its value is determined by the size, shape, and distribution (relative position) of roughness elements. There are several methods for estimating the roughness length [1,3]; however, the fields of application and data requirements of different methods vary.

Roughness length ($z_0$) can be calculated in the following steps.

$$z_0 = (h - z_d)exp\left(-\frac{\kappa}{\sqrt{0{,}5 \cdot C_D \cdot \lambda_F}}\right) \quad \text{(Eq. 6)}$$

where h is the average height weighted by volume, $z_d$ is the thickness of the roughness layer, $C_D$ is the drag coefficient (0,8) and $\lambda_F$ is the frontal area.

By substituting the coefficients, we can obtain a simpler form of the equation [49]:

$$z_0 = (h - z_d)exp\left(-\sqrt{\frac{0{,}4}{\lambda_F}}\right) \quad \text{(Eq. 7)}$$

To determine $z_0$ calculate the average height weighted with the volume:

$$h = \frac{\sum_{i=i}^{n} h_i \cdot V_i}{\sum_{i=1}^{n} V_i} \quad \text{(Eq. 8)}$$

where $h_i$ is the height of the i-$_{th}$ object in a given unit of area and $V_i$ is the volume of the i-$_{th}$ object.

The frontal area can be calculated as follows:

$$\lambda_F(\Theta) = \frac{\sum_{i=1}^{n} A_{Fi}}{A_T} \quad \text{(Eq. 9)}$$

where $A_{Fi}$ is the frontal area of the i-$_{th}$ object, $A_T$ is the area of the studied surface (in the case of multiple directions of the area of the sector concerned), and Θ is the direction of the air flow.

The thickness of the roughness layer can be calculated using the following equation:

$$z_d = h \cdot (\lambda_P)^{0,6} \qquad \text{(Eq. 10)}$$

where:

$$\lambda_P = \frac{\sum_{i=1}^{n} A_{Pi}}{A_T} \qquad \text{(Eq. 11)}$$

$A_{Pi}$ is the area of the i-$_{th}$ object.

The following values can be found for the roughness lengths of different surface types in the literature.

228 **Table 2.** Dependence of Roughness length ($z_0$) on the type of surface [34,38,50]

| **Surface type** | **Roughness length $z_0$ (m)** |
|---|---|
| Very smooth ice, mud | 0.00001 |
| Calm open sea | 0.0002 |
| Wavy open sea | 0.0005 |
| Snow | 0.003 |
| Grassland | 0.008 |
| Pastureland | 0.01 |
| Plough land | 0.03 |
| Perennial plants low bush | 0.05 |
| Rare trees | 0.1 |
| Forest with scattered buildings and other roughness elements | 0.25 |
| Mature forest or settlement with small differences in height | 0.5 |
| Suburb or forest with medium differences in height | 1.5 |
| Downtown, irregular forest area with strongly varying heights | 3.0 |

229

230 **2.1.2.2 Method for the estimation of frontal area index ($\lambda_F$) utilizing UAS-based aerial survey**

231

232 One of the most complex parts of the determination of roughness length is the calculation of the frontal
233 area index ($\lambda_F$). A combination of GIS and UAS-based aerial survey methods were used for this purpose
234 in the frame of the present study.

High-resolution geospatial data acquired through a UAS-based aerial survey were used to accurately compute the Frontal Area Index ($\lambda_F$). Data collection was performed using a DJI Matrice M210 RTK v2 UAS equipped with a Zenmuse X7 24 mm ASPH lens. The flight plan was executed using the DJI Pilot application, which delineated a circular area of interest with a radius of 475 m. Image acquisition was conducted at an altitude of 120 m above ground level, maintaining a 70% overlap for both the front and side laps.

Precise exterior orientation was achieved through Post-Processing Kinematic (PPK) correction of the image coordinates. This correction was facilitated by the combined operation of the DJI D-RTK2 base station and an Emlid Reach RS2 GNSS device, which logged the correction coordinates to differentially refine orientation accuracy. PPK processing was conducted using the original imagery from Emlid Studio. The aerial survey yielded 604 images, each with an approximate ground sampling distance (GSD) of 2.5 cm. Structure-from-motion processing was performed in Agisoft Metashape Professional v2.0 to generate the Digital Surface Model and orthomosaic. The resulting spatial resolutions were 4.7 and 5.2 cm per pixel, respectively.

The $\lambda_F$ calculation process was initiated by creating a vector mask comprising eight circular sectors, each representing one of the eight cardinal directions. This mask was used to clip the DSM. The radius of the circle was adjusted to the study area, which was 475 m. The surface elevation statistics (mean, minimum, maximum, and standard deviation) of the sectors and the volume values of the surface objects were calculated. Cross-sections were obtained starting from the wind measurement station and composing equal-length cross-sections every 10 m per circular sector perpendicular to the cardinal directions. This resulted in 47 cross-sections in each sector. The elevation profile of each cross-section was then calculated. The entire process was implemented and automated in Model Builder, ESRI ArcGIS Desktop v10.8.1 software (ESRI, Redlands, CA, United States).

The transect profiles consisted of the height (h) and distance (x) along the transect line for each vertex of the cross-sectional lines. These data were imported into Microsoft Excel, and we developed a function to determine the maximum height values ($h_i$) at every distance within the stacked profiles. By utilizing the minimal height of the sector and applying this function, it is possible to identify the outermost extent of surface objects in one direction. Ultimately, our method provides a semi-automated solution for calculating the area within the stack profile in each circular sector, specifically the Frontal Area Index ($\lambda_F$).

Our spatial analysis did not consider elevation differences because of the negligible slope of the study area. In areas characterized by significant relief, adaptation is necessary, particularly when employing the normalized digital surface model (nDSM) as the primary dataset, which represents the height of features above ground, rather than the elevation of features relative to the mean sea level or an ellipsoid. The creation of such a dataset would pose significant challenges if only RGB imagery and SfM processing are employed; thus, a LiDAR (Light Detection and Ranging) survey would be indispensable. The computation of the area beneath the curve of the stacked elevation profiles does not rely on integration, because of the absence of profiles described by continuous functions.

### 2.2 Approaching empiric frequency distribution of windspeeds using the Weibull distribution

It is important to know the frequencies of the wind speed classes, especially those that are suitable for wind power generation. Many statistical and energetic parameters can be obtained by approaching the frequency distribution of empirical wind data. Weibull, Rayleigh, normal, lognormal, and gamma distributions are among the statistical distribution functions suitable for this purpose [51–53], from which the two-parameter Weibull distribution is most frequently applied in wind energetics and wind climatology.

The Weibull distribution is advantageous for this purpose because its parameters are relatively easy to estimate from empirical datasets, making it possible to describe the frequency distribution of wind speeds for multiple height levels.

The density function of the simplest form of the Weibull distribution function can be written as follows [51,54]:

$$f(x) = f(x;k;c) = \frac{k}{c}\left(\frac{x}{c}\right)^{k-1} e^{-\left(\frac{x}{c}\right)^{k}} \qquad \text{(Eq. 12)}$$

where $k$ is the shape parameter without dimensions, and $c$ is the scale parameter (m/s). Both can be calculated from a database of the measured wind speeds.

The k – shape and c-scale parameters can be estimated based on the lower and upper quartiles ($q_1$ and $q_3$) and the median ($q_2$) of the wind speed [51,54,55].

This can be calculated as follows:

$$k = \frac{\ln\left(\frac{\ln 0.25}{\ln 0.75}\right)}{\ln\left(\frac{q_3}{q_1}\right)} = \frac{1.573}{\ln\left(\frac{q_3}{q_1}\right)} \qquad \text{(Eq. 13)}$$

$$c = \frac{q_2}{\ln(2)^{\frac{1}{k}}} \qquad \text{(Eq. 14)}$$

### 2.3 Wind energy potential estimation

Wind power estimation with an approach using the Weibull distribution is possible because if wind speed can be characterized by a k- and c-parameter Weibull distribution, then $v_m$ can be characterized by a $k_m$ and $c_m$ parameter Weibull distribution [52,55,56].

#### 2.3.1 Specific wind power estimation using the gamma (Γ) function (W-G)

The specific wind power ($P_f$) using the gamma function (Γ) can be calculated using the following equation [55,57,58]:

$$P_f = \frac{1}{2}\rho c^3 \Gamma\left(1+\frac{1}{k}\right) \quad \text{(Eq. 15)}$$

where c and k are the parameters of the Weibull distribution and ρ is the density of air.

### 2.3.2 Specific wind power estimation using frequency distribution (W-RF)

Another method for specific wind power estimation is to calculate the relative frequency distributions at different height levels [55].

$$P_f = \frac{1}{2}\rho \sum_{i=1}^{n} v_i^3 p_i \quad \text{(Eq. 16)}$$

where $v^3$ -s are the cubes of the centers ($v_i$) of the wind-speed intervals (Δx=1 m/s), $p_i$ s are their cumulative relative frequencies, and n is the number of wind-speed intervals.

### 2.3.3 The Windographer software specific wind power estimation methodology (Windog)

Windographer calculates the wind power density at each time step using the following equation:

$$\frac{P}{A} = \frac{1}{2}\rho U^3 \quad \text{(Eq. 17)}$$

where $P/A$ is the wind power density, or the power per unit area, within the time step [W/m$^2$]; $\rho$ is the air density within the time step [kg/m$^3$]; $U$ is the average wind speed within the time step [m/s].

## 3. Results and discussion

The first step in the wind energy potential evaluation of a site is the wind climate description, which includes statistical analyses of the wind speeds and wind directions. However, it is important to have exact knowledge of both characteristics of wind-field wind-speed statistics, which have accentuated importance from energetic aspects. It is evident from the methods discussed in the previous section that the potential wind power is proportional to the cube of the wind speed, which is a slight change in wind speed, resulting in a significant alteration in the potential wind power.

### 3.1. Analyses of empiric wind speed data

First, an analysis of the empirical wind speed data was conducted. As shown in Figure 3, there was an increase in the mode of the wind speed intervals parallel to increasing height up to 90 m (20 m – 2-3 m/s; 50 m – 3-4 m/s; 80 and 90 m – 4-5 m/s). The mode drops and falls in the 3-4 m/s wind speed class at heights between 90 m and 120 m. The frequencies of wind speed classes over the 3-4 m/s class, which is characteristic for lower levels, show a moderate decrease; the relative frequency of the 9-10 m/s wind speed class is 4.8% at 100 m, 5.7% at 110 m, and 6.3% at 120 m. From an energetic perspective, wind speed classes over 3 m/s are relevant, since the cut in speed of industrial-scale wind turbines is around this value, depending on the type.

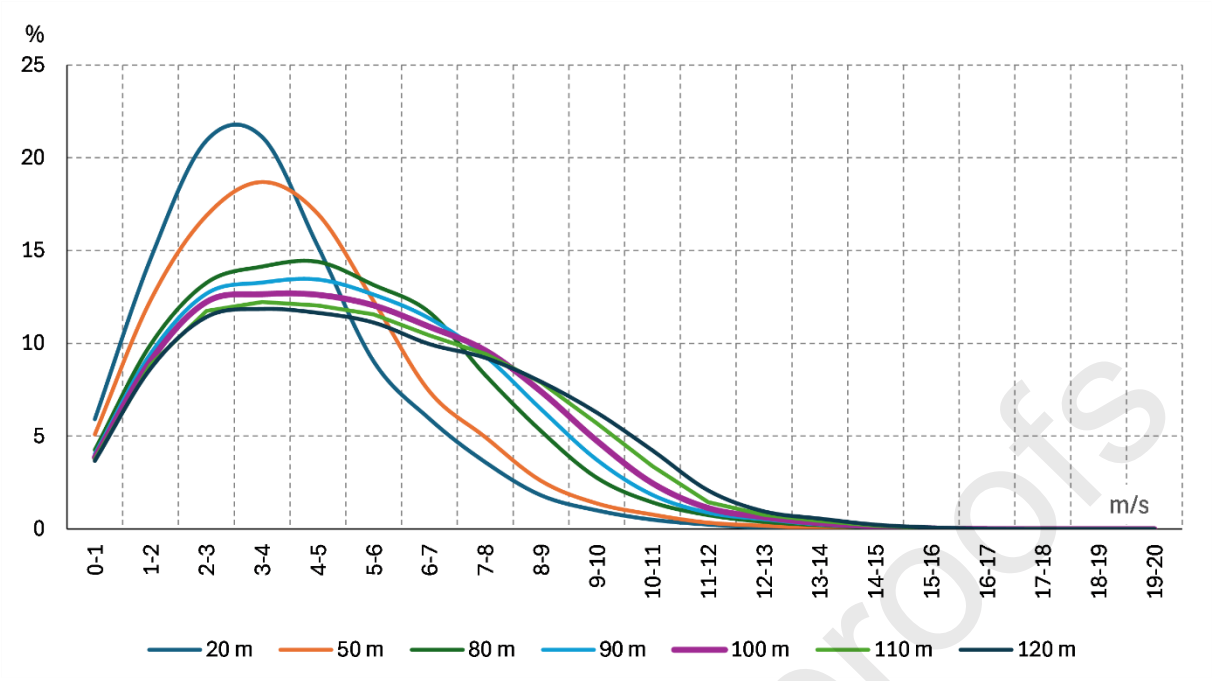


Fig. 3. Relative frequencies (%) of the empiric wind speeds (m/s) of the height levels involved in the study.

The estimation techniques are described in Section 2.1. A comparative statistical analysis was performed on the datasets obtained using methods V1 and V2. By applying these methods, datasets with a temporal resolution of 10 min are produced, making it possible to detect spatial and temporal patterns.

Differences between the empirical and extrapolated data were first analyzed on a monthly/diurnal scale. Figure 4 shows the differences in wind speeds extrapolated for the 80- and 120-meter height levels using methods V1 and V2. There were no significant differences between the two methods at either height. The isopleth diagrams of the differences showed the same pattern for both methods at both heights. Gualtieri found similar diurnal and annual courses for methods V1 and V2, in accordance with the results of the present study [43]. Differences appeared in the pattern of positive and negative differences at heights of 80 m and 120 m for the entire dataset. The ratios of overestimation and underestimation between the V1 and V2 extrapolated and empirical data are shown in Table 3.. Underestimation was dominant, with a frequency of over 70% for both the methods and heights. As shown in Figure 4, the degree of overestimation was nearly twice as high as that of underestimation at both heights. The period of overestimation was most emphasized at 120 m in the first five months of the year.

**Table 3.** The ratio of over and underestimation between V1, V2 extrapolated and empirical data

| | V1 | | V2 | |
|---|---|---|---|---|
| | Overestimation | Underestimation | Overestimation | Underestimation |
| 80 m | 16.2% | 83.8% | 23% | 77% |

| | | | | |
|---|---|---|---|---|
| 120 m | 24.6% | 75.4% | 29.6% | 70.4% |

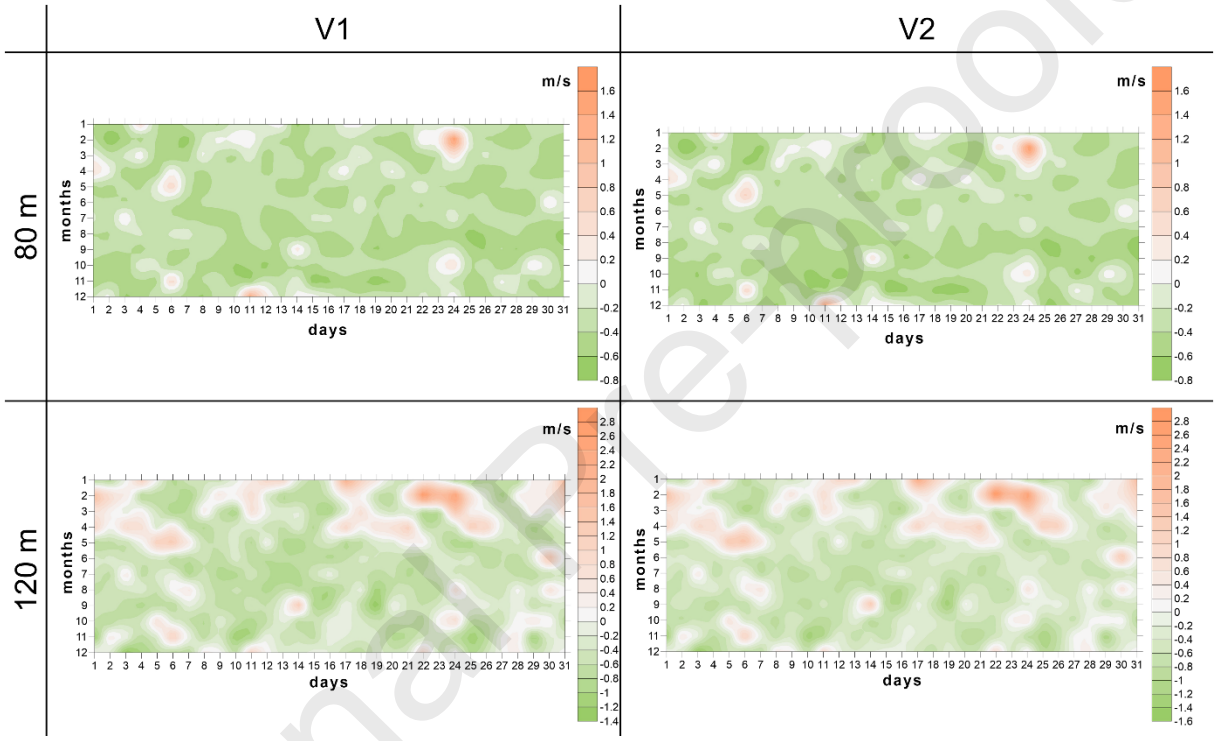


Fig. 4. Differences between the empiric and estimated wind speeds using method V1 and V2 at heights of 80 and 120 m on a monthly/diurnal scale.

The results from methods V1 and V2 showed a different but more characteristic pattern in another timeframe. The comprehension of the two methods on an annual/diurnal timescale is shown in Figure 5. A similar annual/diurnal course of the power-law exponent was reported in a previous study [39]. In a study published in 2018, Gualtieri found insignificant differences in the patterns of power-law exponents estimated at several height levels [42]. The degree and sign of overestimation and underestimation are determined mainly by atmospheric stability conditions. The largest differences were underestimations, which occurred during the night period under stable conditions, and there were no significant differences in the ratio of under- and over-estimations in the case of methods V1 and V2 at 80 m. However, in the case of method V2, the stable and unstable periods were more clearly separated. The differences between the empirical and estimated wind speeds were more pronounced at 120 m. Overestimation was more frequent in the first half of the year for both the methods at 120 m. In the case of Method V2, overestimation was emphasized more during the day. Underestimation is characteristic of the hours around sunrise and sunset at this height, when the solar energy input into the atmosphere starts and ends. Gualtieri found similar diurnal and annual courses for methods V1 and V2, which is in agreement with the findings of the present study [42].

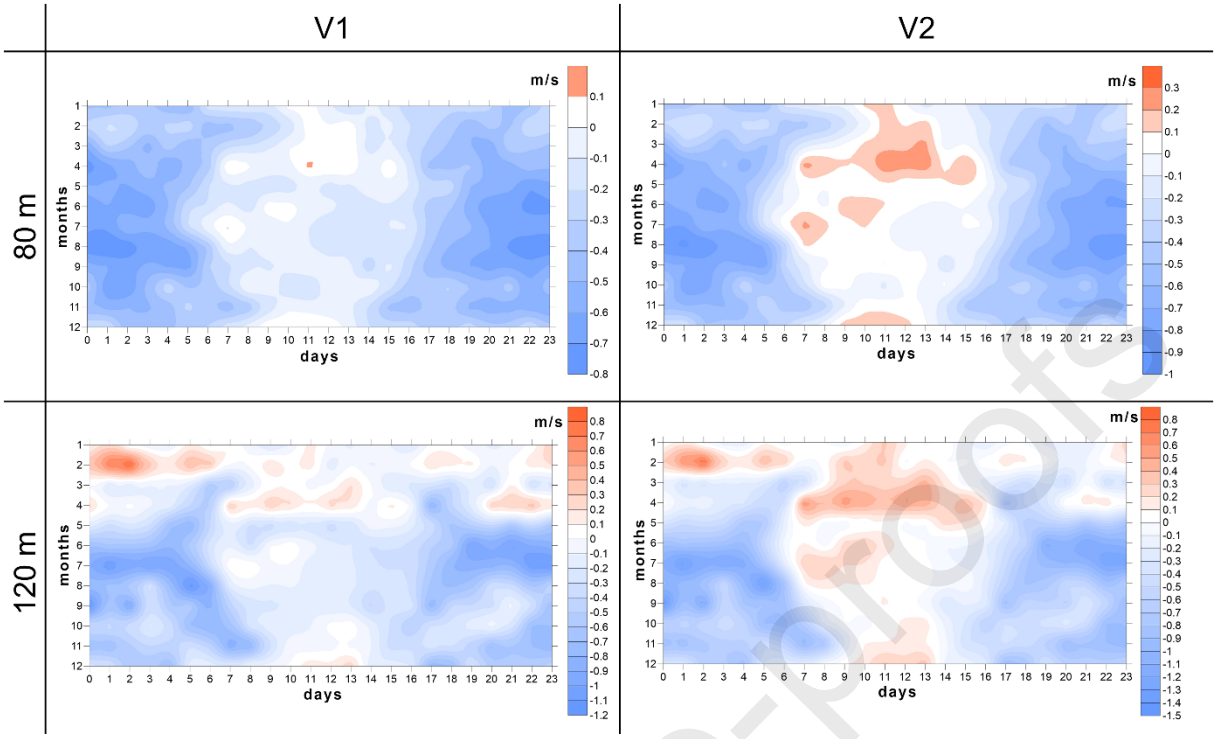


Fig. 5. Differences between the empiric and estimated wind speeds using method V1 and V2 at heights of 80 and 120 m on an annual/diurnal scale.

Differences between the empirical and estimated wind speeds for the 80 and 120 levels from methods V1 and V2 were analyzed in a temporal/spatial context in the following unit. The complexity of the environment at a measurement site is important. The orography, size, shape, and distribution (relative position) of roughness elements are important characteristics. These are static factors during a year from the aspect of their effects on the moving air, while vegetation shows seasonal changes in height, density, etc., which result in seasonal differences in the resistance of the surface to airflow. The results of the comprehension of methods V1 and V2 at the 80- and 120-meters level are presented in Figure 6. Only minor differences were observed between the empirical and estimated wind speeds. Moreover, the differences were the smallest at both heights. There was a significant discrepancy in the under/overestimation ratios between heights. This ratio was 1/10 at 80 m and 1/5 at 120 m. Gualtieri found significant differences in the spatial pattern of the power-low exponent and z0 values by direction in the case of two of three sites in a study published in 2011, which can be explained by the differences in the combined effect of the roughness objects on the surface [43].

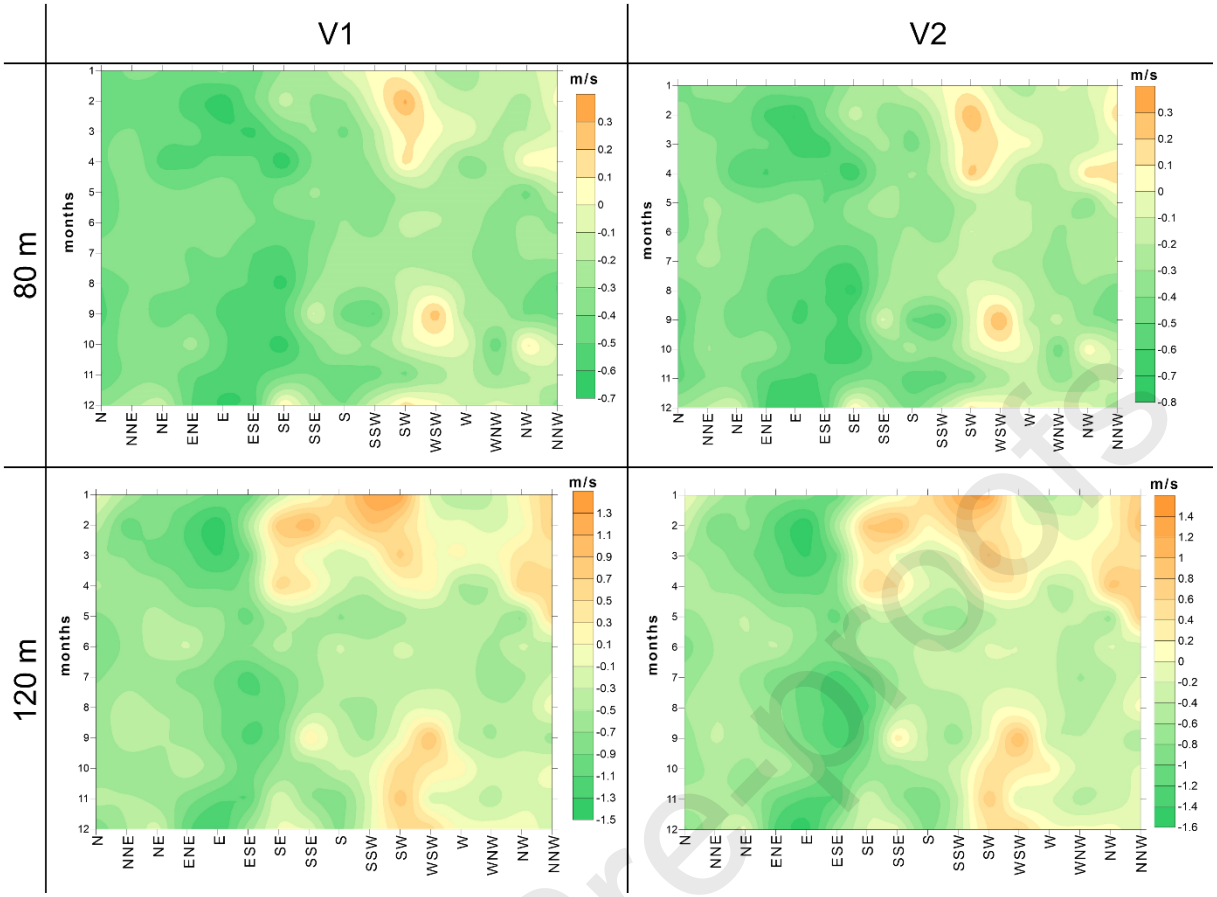


Fig. 6. Differences of the measured and estimated wind speeds by methods V1 and V2 for the heights of 80 and 120 m in a month/direction context.

The root mean square error (RMSE) values of the differences calculated for the heights involved in the study are presented in Figure 7. It is evident from the figure that there are only slight differences between methods V1 and V2. However, it is clear that the wind speeds estimated by V1 were closer to the measured wind speeds at both heights. Naturally, the uncertainty in the estimation increases with increasing height. The increase in uncertainty can be considered approximately linear, even though the increase in wind speed with height is nonlinear.

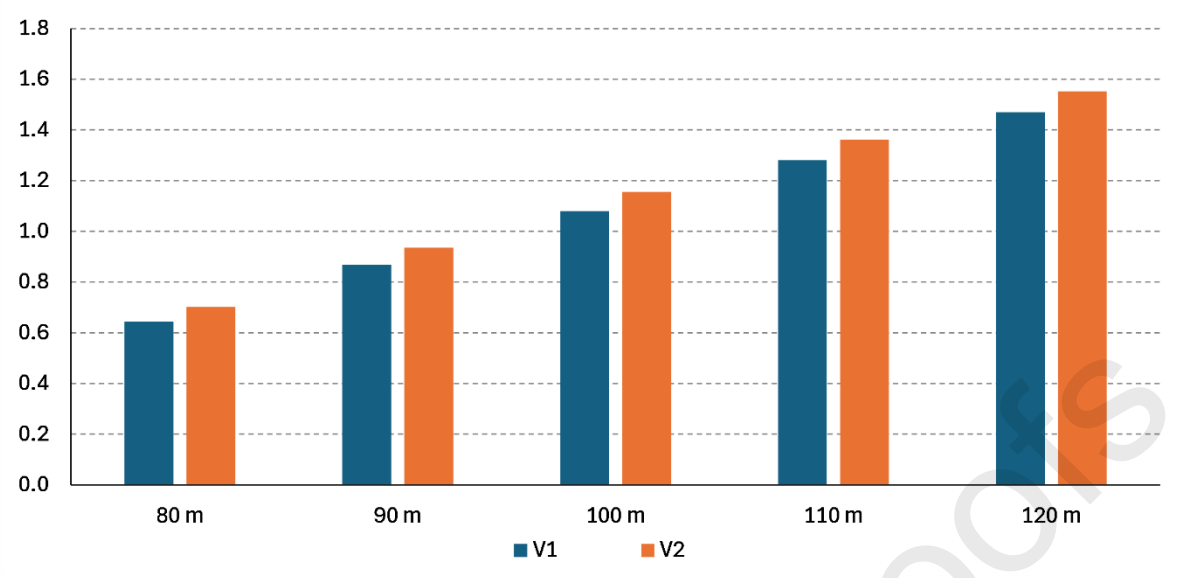


Fig. 7. RMSE values of the differences of the empiric and estimated wind speeds by methods V1 and V2 between the 80 m and 120 m levels.

In the final section, the techniques presented in Section 2.3. available for the estimation of the specific wind power potential from the perspective of the differences in the estimated wind power potential. Wind power determined using the wind speeds estimated by methods V1 and V2 was compared to specific potential values estimated from the empirical wind speed data and to values calculated using Windographer software. Wind power was estimated in 10-meter steps for height levels between 80 and 120 m, as in the previous sections. The results are shown in figure 7.

The algorithm for the potential calculation in the case of methods V1, V2, and W-RF is the same. The details of this method are presented in Section 2.3. Small and insignificant differences were observed between the estimations of the three methods at a given height level. Although the three estimation methods were identical, Weibull distribution was used in the W-RF method. First, the shape and scale parameters of the Weibull distribution were determined from empirical data, and then the specific values of the different wind speed intervals were calculated and summarized.

The results for the W group were calculated using the estimation method described in section 2.3. The specific wind power at different height levels had a higher standard deviation than those in the previously presented cases. The standard deviation of the estimated specific wind power at different height levels is higher than that in the previous cases; however, there are small differences only in this case.

The last group shows the values calculated using the Windographer software. The estimation method for the software is described in detail in Section 2.3.3. All the methods involved in this study underestimated the specific wind power for each height level [47,59].

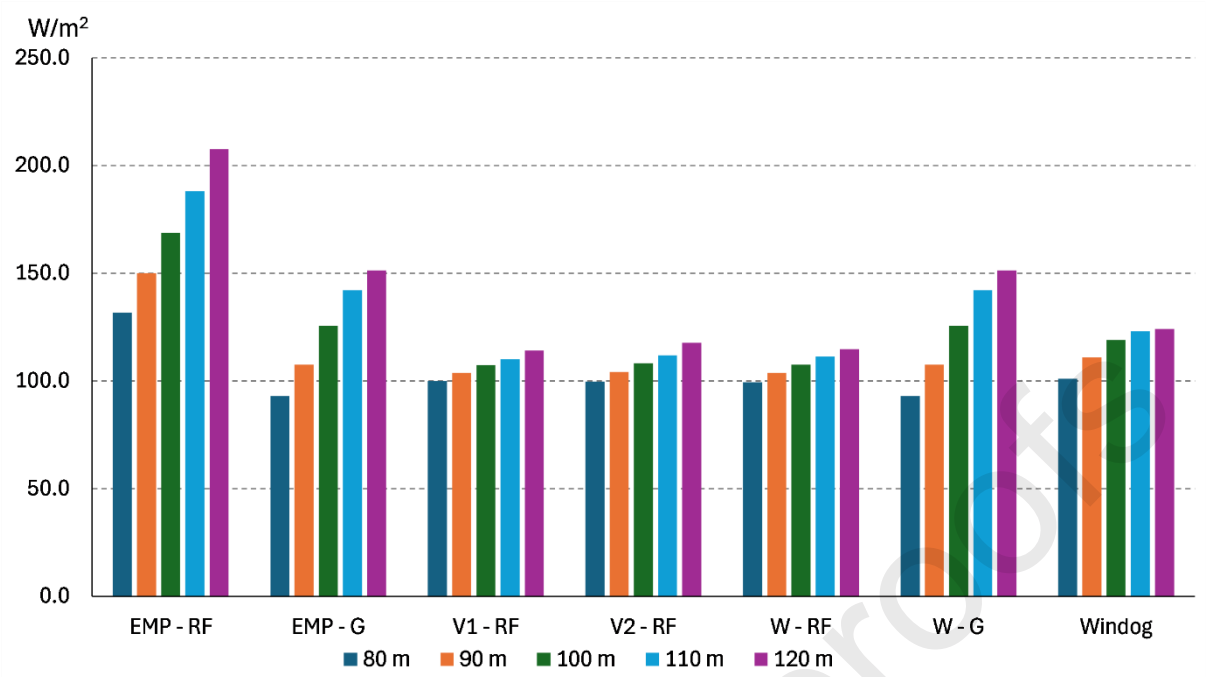


Fig. 8. Specific wind power values estimated with the different methods (EMP-RF – **empiric** – *method W-RF*; EMP - G – **empiric** – *method W-G*; V1-RF – **V1** – *method W-RF*; V2-RF – **V2** – *method W-RF*; W-RF – **Weibull-distribution –** *method W-RF*; W-G – **Weibull-distribution shape and scale parameters determined by the quartile methods** – *method W*; Windog – **empiric** – *specific potential calculated by the Windographer software method*; legend: name of the method abbreviation – **source of data/wind speed estimation method** – *potential estimation method*) [16,43]

## 4. Conclusions

Wind speeds measured at 50 m were extrapolated for height levels of 80, 90, 100, 110, and 120 m using dynamic power law exponent values. A comparative statistical analysis of the datasets of methods V1 and V2 in monthly/diurnal, annual/diurnal, and month/direction contexts showed no significant differences between the two methods at either height level. Differences appeared in the pattern of positive and negative differences at heights of 80 m and 120 m for the entire dataset. Underestimation was dominant, with a frequency of over 70% for both the methods and heights. Wind power was determined using the power law (method V1), roughness length (method V2), frequency distribution (method W-RF), and gamma distribution (method W-G), and Windographer software was compared to the values calculated from the empirical (measured) wind speeds. There were no significant differences between the estimations obtained using different methods. All methods involved in the study underestimated the wind speeds and wind energy potential for each height level; consequently, methods V1 and V2 could be used alternatively, depending on the input data available for the analyses. On this basis, the present work can help identify the most adequate method for analysis. The major advantage of method V2 is that it provides the same accuracy as V1, which requires a UAS-based aerial survey at the beginning, but continuous wind measurements must be performed at a lower height only. This means that there is no need for a high measurement tower that the measurements are simpler and more cost effective and cause much less disturbance to the environment. Another important advantage of the methods presented here is that they use a dynamic approach of power law exponent values that provide a more realistic estimation of wind speed and energy on a diurnal scale.

The comparative study presented in detail highlights the differences between the methods, particularly regarding their input data requirements. Depending on the potential of a study area (terrain, accessibility,

legal regulations in the immediate vicinity of built-up or inhabited settlements, available means, financial resources), the method can be adapted to the following circumstances:

- The construction and operation of a measurement tower (at least 50 m high, measurement should be at least two different heights, e.g., 20 m and 50 m); this is the toolbox of the V1 method.
- The construction and operation of a measuring tower (at least 20 m high; the measurement must be made at one height, e.g., 20 m), but also a DSM by UAS will be required to measure the aerodynamic roughness; this is the toolbox of method V2.

Although the V2 method measured a higher RMSE value than the V1 method at all tested heights, the result of the specific wind energy potential estimation showed a nearly equal value; thus, it can be stated that the V2 method requires a lower financial investment (considering that it requires the construction and operation of a measuring tower of at least 50 m, because its height requires several permits before commissioning).

## Declaration of Competing Interest

The Authors declare that they have no known competing financial interests or personal relationships that could influence the work reported in this study.

## Acknowledgements

Project no. TKP2021-NKTA-34 was implemented with support provided by the Ministry of Innovation and Technology of Hungary from the National Research, Development and Innovation Fund, financed under the TKP2021-NKTA funding scheme. During the preparation of this work, the author(s) used the Paperpal: AI Academic Writing Tool to improve the English of the manuscript. After using this tool/service, the authors reviewed and edited the content as required and took full responsibility for the content of the publication.

## References

[1] Zhang C, Yuan Y, Zou X, Wang H, Li Q, Wang Z, et al. A comparison of the aerodynamic characteristics of four kinds of land surface in wind erosion areas of northern China. CATENA 2022;212:106112. https://doi.org/10.1016/j.catena.2022.106112.

[2] Grimmond CSB, OKE TR. Aerodynamic Properties of Urban Areas Derived from Analysis of Surface Form. J Appl Meteorol 1998;38:1262–92.

[3] Gál T, Unger J. Detection of ventilation paths using high-resolution roughness parameter mapping in a large urban area. Build Environ 2009;44:198–206. https://doi.org/10.1016/j.buildenv.2008.02.008.

[4] Fan MY, Li WJ, Luo XL, Shui QX, Jing LZ, Gu ZL, et al. Parameterised drag model for the underlying surface roughness of buildings in urban wind environment simulation. Build Environ 2022;209:108651. https://doi.org/10.1016/j.buildenv.2021.108651.

[5] Bhatt MM, Gupta K, Danodia A, Chakroborty SD, Patel NR. Detailed urban roughness parametrization for anthropogenic heat flux estimation using earth observation data. Heliyon 2023;9:e18361. https://doi.org/10.1016/j.heliyon.2023.e18361.

[6] Kato S, Yamaguchi Y. Analysis of urban heat-island effect using ASTER and ETM+ Data: Separation of anthropogenic heat discharge and natural heat radiation from sensible heat flux. Remote Sens Environ 2005;99:44–54. https://doi.org/10.1016/j.rse.2005.04.026.

[7] Hou H, Su H, Yao C, Wang Z-H. Spatiotemporal patterns of the impact of surface roughness and morphology on urban heat island. Sustain Cities Soc 2023;92:104513. https://doi.org/10.1016/j.scs.2023.104513.

[8] Nickerson EC, Smiley VE. Surface Layer and Energy Budget Parameterizations for Mesoscale Models. J Appl Meteorol Climatol 1975;14:297–300. https://doi.org/10.1175/1520-0450(1975)014<0297:SLAEBP>2.0.CO;2.

[9] Touma JS. Dependence of the Wind Profile Power Law on Stability for Various Locations. J Air Pollut Control Assoc 1977;27:863–6. https://doi.org/10.1080/00022470.1977.10470503.

[10] Vasaturo R, Kalkman I, Blocken B, van Wesemael PJV. Large eddy simulation of the neutral atmospheric boundary layer: performance evaluation of three inflow methods for terrains with different roughness. J Wind Eng Ind Aerodyn 2018;173:241–61. https://doi.org/10.1016/j.jweia.2017.11.025.

[11] Bahamonde MI, Litrán SP. Study of the energy production of a wind turbine in the open sea considering the continuous variations of the atmospheric stability and the sea surface roughness. Renew Energy 2019;135:163–75. https://doi.org/10.1016/j.renene.2018.11.075.

[12] European Wind Energy Association, editor. European Wind Energy Conference & Exhibition 2011 (EWEC 2011): Brussels, Belgium, 14 - 17 March 2011. Red Hook, NY: Curran; 2012.

[13] Fernández-Cabán PL, Masters FJ. Near surface wind longitudinal velocity positively skews with increasing aerodynamic roughness length. J Wind Eng Ind Aerodyn 2017;169:94–105. https://doi.org/10.1016/j.jweia.2017.06.007.

[14] Liu Y, Qiao Y, Han S, Tao T, Yan J, Li L, et al. Rotor equivalent wind speed calculation method based on equivalent power considering wind shear and tower shadow. Renew Energy 2021;172:882–96. https://doi.org/10.1016/j.renene.2021.03.089.

[15] Batablinlè L, Bazyomo SD, Badou FD, Jean H, Hodabalo K, Zakari D, et al. Climate, water, hydropower, wind speed and wind energy potential resources assessments using weather time series data, downscaled regional circulation models: A case study for Mono River Basin in the Gulf of Guinea region. Renew Energy 2024;224:120099. https://doi.org/10.1016/j.renene.2024.120099.

[16] Hasan M, Dey P, Janefar S, Salsabil NA, Khan IJ, Chowdhury N-U-R, et al. A critical analysis of wind energy generation potential in different regions of Bangladesh. Energy Rep 2024;11:2152–73. https://doi.org/10.1016/j.egyr.2024.01.061.

[17] Rekik S, El Alimi S. Optimal wind-solar site selection using a GIS-AHP based approach: A case of Tunisia. Energy Convers Manag X 2023;18:100355. https://doi.org/10.1016/j.ecmx.2023.100355.

[18] Liu F, Sun F, Wang X. Impact of turbine technology on wind energy potential and CO2 emission reduction under different wind resource conditions in China. Appl Energy 2023;348:121540. https://doi.org/10.1016/j.apenergy.2023.121540.

[19] Xiaoxia G, Luqing L, Shaohai Z, Xiaoxun Z, Haiying S, Hongxing Y, et al. LiDAR-based observation and derivation of large-scale wind turbine's wake expansion model downstream of a hill. Energy 2022;259:125051. https://doi.org/10.1016/j.energy.2022.125051.

[20] dos Santos FS, do Nascimento KKF, da Silva Jale J, Xavier SFA, Ferreira TAE. Brazilian wind energy generation potential using mixtures of Weibull distributions. Renew Sustain Energy Rev 2024;189:113990. https://doi.org/10.1016/j.rser.2023.113990.

[21] Kang S, Khanjari A, You S, Lee J-H. Comparison of different statistical methods used to estimate Weibull parameters for wind speed contribution in nearby an offshore site, Republic of Korea. Energy Rep 2021;7:7358–73. https://doi.org/10.1016/j.egyr.2021.10.078.

[22] Irwin JS. A theoretical variation of the wind profile power-law exponent as a function of surface roughness and stability. Atmospheric Environ 1967 1979;13:191–4. https://doi.org/10.1016/0004-6981(79)90260-9.

[23] Gualtieri G. Atmospheric stability varying wind shear coefficients to improve wind resource extrapolation: A temporal analysis. Renew Energy 2016;87:376–90. https://doi.org/10.1016/j.renene.2015.10.034.

[24] DeMarrais GA. WIND-SPEED PROFILES AT BROOKHAVEN NATIONAL LABORATORY. J Atmospheric Sci 1959;16:181–90. https://doi.org/10.1175/1520-0469(1959)016<0181:WSPABN>2.0.CO;2.

[25] Panofsky HA, Blackadar AK, McVehil GE. The diabatic wind profile. Q J R Meteorol Soc 1960;86:390–8. https://doi.org/10.1002/qj.49708636911.

[26] Draxl C, Hahmann AN, Peña A, Giebel G. Evaluating winds and vertical wind shear from Weather Research and Forecasting model forecasts using seven planetary boundary layer schemes. Wind Energy 2014;17:39–55. https://doi.org/10.1002/we.1555.

[27] Lázár I, Csákberényi-Nagy G, Túri Z, Kapocska L, Tóth T, Tóth J. Analysis of factors affecting wind-energy potential in low built-up urban environments. 2014. https://doi.org/10.13140/2.1.4231.5200.

[28] Wieringa J. How far can agrometeorological station observations be considered representative? Prepr 23rd Am Meteor Soc Conf Agric. For. Meteorol. Albuq. J15, 1998, p. 9–12.

[29] Tamura Y, Suda K, Sasaki A, Miyashita K, Iwatani Y, Maruyama T, et al. Simultaneous wind measurements over two sites using Doppler sodars. J Wind Eng Ind Aerodyn 2001;89:1647–56. https://doi.org/10.1016/S0167-6105(01)00149-0.

[30] Shah Irshad A, Kargar N, Elkholy MH, Ahmad Ludin G, Elias S, Hilali A, et al. Techno-economic evaluation and comparison of the optimal PV/Wind and grid hybrid system with horizontal and vertical axis wind turbines. Energy Convers Manag X 2024;23:100638. https://doi.org/10.1016/j.ecmx.2024.100638.

[31] Aujeszky L. Meteorológiai előmunkálatok a magasépítésben végzendő szélterhelés számításokhoz. J Hung Meteorol Serv 1949;53:15–25.

[32] Antoniou I, Pedersen SM, Enevoldsen PB. Wind Shear and Uncertainties in Power Curve Measurement and Wind Resources. Wind Eng 2009;33:449–68. https://doi.org/10.1260/030952409790291208.

[33] Counihan J. Adiabatic atmospheric boundary layers: A review and analysis of data from the period 1880–1972. Atmospheric Environ 1967 1975;9:871–905. https://doi.org/10.1016/0004-6981(75)90088-8.

[34] Bañuelos-Ruedas F, Angeles-Camacho C, Rios-Marcuello S, Bañuelos-Ruedas F, Angeles-Camacho C, Rios-Marcuello S. Methodologies Used in the Extrapolation of Wind Speed Data at Different Heights and Its Impact in the Wind Energy Resource Assessment in a Region. Wind Farm - Tech. Regul. Potential Estim. Siting Assess., IntechOpen; 2011. https://doi.org/10.5772/20669.

[35] Tse KT, Li SW, Chan PW, Mok HY, Weerasuriya AU. Wind profile observations in tropical cyclone events using wind-profilers and doppler SODARs. J Wind Eng Ind Aerodyn 2013;115:93–103. https://doi.org/10.1016/j.jweia.2013.01.003.

[36] Kornélia R. A szélenergia hasznosításának lehetőségei Magyarországon : hazánk szélklímája, a rendelkezésre álló szélenergia becslése és modellezése. 2004.

[37] Tar K. A legmegbízhatóbb Hellmann-kitevő meghatározásának statisztikai módszere. Acta Climatol 2016;50/B:129–38.

[38] Masters GM. Renewable and Efficient Electric Power Systems 2004. https://doi.org/10.1002/0471668826.

[39] Lázár I, Tóth T, Sándor S. A potenciális szélenergiát meghatározó terepi érdesség vizsgálata távérzékelt szélsebesség adatok alapján. Tanulmköt. Prof Dr Mika János Szül. 70 Évfordulója Alkalmából, Eger: Eszterházy Károly Katolikus Egyetem; 2023, p. 241–58.

[40] Mojumder MdFH, Islam T, Chowdhury P, Hasan M, Takia NA, Chowdhury N-U-R, et al. Techno-economic and environmental analysis of hybrid energy systems for remote areas: A sustainable case study in Bangladesh. Energy Convers Manag X 2024;23:100664. https://doi.org/10.1016/j.ecmx.2024.100664.

[41] Gualtieri G. A comprehensive review on wind resource extrapolation models applied in wind energy. Renew Sustain Energy Rev 2019;102:215–33. https://doi.org/10.1016/j.rser.2018.12.015.

[42] Gualtieri G. Surface turbulence intensity as a predictor of extrapolated wind resource to the turbine hub height: method's test at a mountain site. Renew Energy 2018;120:457–67. https://doi.org/10.1016/j.renene.2018.01.001.

[43] Gualtieri G, Secci S. Wind shear coefficients, roughness length and energy yield over coastal locations in Southern Italy. Renew Energy 2011;36:1081–94. https://doi.org/10.1016/j.renene.2010.09.001.

[44] Ngila Mulumba A, Farzaneh H. Techno-economic analysis and dynamic power simulation of a hybrid solar-wind-battery-flywheel system for off-grid power supply in remote areas in Kenya. Energy Convers Manag X 2023;18:100381. https://doi.org/10.1016/j.ecmx.2023.100381.

[45] Bansal RC, Bhatti TS, Kothari DP. On some of the design aspects of wind energy conversion systems. Energy Convers Manag 2002;43:2175–87. https://doi.org/10.1016/S0196-8904(01)00166-2.

[46] Patel M, Beik O. Wind and Solar Power Systems: Design, Analysis, and Operation. Routledge CRC Press n.d. https://www.routledge.com/Wind-and-Solar-Power-Systems-Design-Analysis-and-Operation/Patel-Beik/p/book/9780367476939 (accessed May 2, 2024).

[47] Silva AR, Pimenta FM, Assireu AT, Spyrides MHC. Complementarity of Brazil's hydro and offshore wind power. Renew Sustain Energy Rev 2016;56:413–27. https://doi.org/10.1016/j.rser.2015.11.045.

[48] Gál T. Az összetett vásrosi felszín geometriáját leíró paraméterek számítása és városklimatológiai alkalmazása, 2009.

[49] Bottema M, Mestayer PG. Urban roughness mapping – validation techniques and some first results. J Wind Eng Ind Aerodyn 1998;74–76:163–73. https://doi.org/10.1016/S0167-6105(98)00014-2.

[50] Borja Díaz MA. Estado del arte y tendencias de la tecnología eoloeléctrica. UNAM, Programa Universitario de Energía; 1998.

[51] Tar K. Some statistical characteristics of monthly average wind speed at various heights. Renew Sustain Energy Rev 2008;12:1712–24. https://doi.org/10.1016/j.rser.2007.01.014.

[52] Safari B. Modeling wind speed and wind power distributions in Rwanda. Renew Sustain Energy Rev 2011;15:925–35. https://doi.org/10.1016/j.rser.2010.11.001.

[53] A. Francis F, D. Nalamutt DT. Statistical Analysis of Wind Speed and Evaluation of Wind Power Density for Colaba, Mumbai 2019.

[54] Justus CG, Hargraves WR, Mikhail A, Graber D. Methods for Estimating Wind Speed Frequency Distributions. J Appl Meteorol Climatol 1978;17:350–3. https://doi.org/10.1175/1520-0450(1978)017<0350:MFEWSF>2.0.CO;2.

[55] Hadnagy I. A felszínközeli szélmező energetikai jellemzése Kárpátalján. Beregszász-Ungvár: II: Rákóczi Ferenc Kárpátaljai Magyar Főiskola; 2023.

[56] Azad AK, Rasul MG, Yusaf T. Statistical Diagnosis of the Best Weibull Methods for Wind Power Assessment for Agricultural Applications. Energies 2014;7:3056–85. https://doi.org/10.3390/en7053056.

[57] Troen I, Petersen EL. European wind atlas. Roskilde: Risø National Laboratory; 1989.

[58] Ahmed A, Adisa A, Dandakouta H. An Evaluation of Wind Energy Potential in the Northern and Southern Regions of Nigeria on the Basis of Weibull and Rayleigh Models 2013;1:37–42.

[59] AL Jarrah AM, AL Dwairi RA. Jordan wind energy potential and suggested areas for large-scale wind turbines investment. Energy Sustain Dev 2024;80:101452. https://doi.org/10.1016/j.esd.2024.101452.

Highlights

- Vertical extrapolation of wind speed using power law exponent and roughness lenght
- Comprehesion of wind energy potencial estimation techniques
- Determination of aerodinamical surface roughness
- Empirical vertical wind profile from Doppler SODAR measurement